Modelling of Reduced Electromechanical Interaction System for Aircraft Applications

Constanza Ahumada [1*], *Pat Wheeler* [2]

[1] *Departamento de Ingeniería Eléctrica, Universidad de Chile, Santiago, Chile*
[2] *Faculty of Engineering, University of Nottingham, Nottingham, United Kingdom*
[*] coahumad@ing.uchile.cl

Abstract: Rotational systems, such as aircraft engine drivetrains, are subject to vibrations that can damage shafts. Torsional vibrations in drivetrains can be excited by the connection of loads to the generator due to electromechanical interaction. This problem is particularly relevant in new aircraft, because the drivetrain is flexible and the electrical power system (EPS) load is high. To extend the lifespan of the aircraft engine, the electromechanical interaction must be considered. Since real time constants of the electrical and mechanical systems have very different magnitudes, the simulation time can be high. Furthermore, highly detailed models of the electrical system have unnecessary complexity for the study of electromechanical interactions. For these reasons, modelling using reduced order systems is fundamental. Past studies of electromechanical interaction in aircraft engines developed models that allow the analysis of the torsional vibration, but these are difficult to implement. In this paper, a reduced order electromechanical interaction system for aircraft applications is proposed and validated using experimental results. The proposed system uses a reduced drivetrain, simplified EPS, and sensorless measurement of the vibrations. The excitation of torsional vibrations obtained are compared to past studies to prove that the reduced order system is valid for studying the electromechanical interactions.

1. Introduction

Rotating mechanical systems, such as an aircraft's drivetrain, can be subject to three types of vibrations: axial vibrations, torsional vibrations, and transversal vibrations. The axial vibrations occur along the shaft length axis. The torsional vibrations produce a twist motion around the rotor shaft, and the transversal vibrations or critical speeds cause horizontal and vertical displacements of the rotor [1]. In this paper, the excitation of torsional vibrations due to electromechanical interactions are studied.

Electromechanical interaction has been known since the 70s when the generator shaft of the Mohave generation plant broke due to sustained excitation, which was induced by the electrical system [2]. However, it has been with the introduction of more electric technologies [3] and renewable energies [4, 5] that studies in electromechanical interaction gained importance. Wind turbines, marine vessels, and aircraft systems have more complex control systems [5] and new electrical power loads (such as actuators or pulsating loads) which can be sources of electromechanical interaction [6–8]. Additionally these technologies have size and weight restrictions and higher safety requirements [3, 6, 9]. These characteristics make the study of electromechanical interaction fundamental for transportation systems and renewable energies. Most of the research has focused in the identification of the problem and the modelling of the interaction. For example, in [8, 10] a reduced electromechanical model of marine systems is developed. In [11] torsional vibrations in an induction motor drive are analysed, and in [3, 9, 12] the modelling and identification of the electromechanical interaction in aircraft systems are studied. However, while the study of electromechanical interaction is gaining importance, the models proposed for each application are still complex and the solutions to reduce the excitation of torsional vibration still needs to be studied. This paper studies the electromechanical interaction in aircraft systems.

The electromechanical system of an aircraft is composed of the engine, the mechanical drivetrain, the generator and the electrical power system (EPS), as shown in Fig. 1. Electromechanical interaction can be due to: the connection of electrical loads, which excite transient torsional vibrations on the drivetrain [3]; to the use of a generator control unit (GCU) that does not consider the properties of the aircraft drivetrain, and therefore can produce resonance or make the system unstable because of negative damping effects [3, 6]; or to grid faults, which apply torques higher than the maximum of seven times the nominal torque allowed [1, 13–15]. Moreover, since the engine inertia is high and the shaft is flexible to reduce weight, and because the EPS is large, the likelihood of electromechanical interaction in aircraft systems is high [1].

In the case of electrical load connections, the excitation torque can be impulsive, as in the case of transient loads such as electrohydraulic actuators (EHA) or electromechanical actuators (EMA), or periodic (pulsating loads, high power loads) such as radars [16] . The damage of the torsional vibration on a mechanical component increases, with each oscillation producing small cracks that propagate through the material. The maximum torsional vibration allowed depends on the duration and the amplitude of the stress [17]. For higher amplitude stresses, the number of times the stress can occur reduces [1]. The shaft of a system can sustain damage if the torque applied is higher than the maximum it can stand, which is proportional to the shear stress of the material and the inertia, and inverse to the diameter of the component [1, 18]; or if the maximum sum

of vibrations that it can hold has been reached. Fatigue of the material occurs when the cross-section of the material is lower than the required for the torque applied [1, 19, 20]. The maximum number of oscillations depends upon the rate of decay of them, and hence on the mechanical damping of the shaft system [17].

Since most torsional vibrations are due to systems with a flexible shaft, which are characterised by a low stiffness [1, 18], increasing the stiffness of the drivetrain has been a traditional solution to reduce the torsional vibrations [21]. Higher stiffness can be obtained using shafts with larger diameters, but this is not always sought as also the weight rises. For this reason, in [18] the use of hollow shafts to increase the stiffness while maintaining the weight is presented. However, this method can be expensive in a system with space restrictions as aircraft [22].

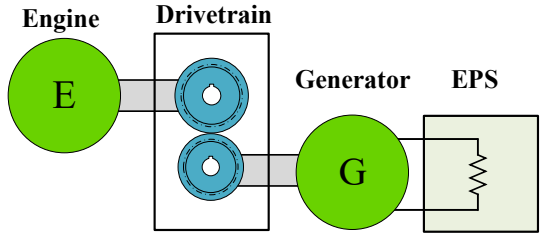

Fig. 1: Electromechanical System Schematic.

To study the electromechanical interactions, the electrical and mechanical systems must be modelled. The presence of low and high natural frequencies in the mechanical and electrical systems respectively implies that simulations take a long time to run [3].

To decrease the complexity of the mechanical model, and hence decrease the number of equations and simulation time, the mechanical drivetrain can be reduced to be represented only by the natural frequencies responsible for the torsional vibrations that are being excited by electromechanical interaction [1, 3, 8]. In the case of aircraft systems only two studies, carried out by T. Feehally in [3] and G. Moore in [23], have analysed the reduction of the aircraft drivetrain. These studies showed that the engine drivetrain could be reduced from 9 to 3 natural frequencies. This paper further reduces the work presented in [3, 23] and introduces a two natural frequency model, with values close to the responsible for the torsional vibrations of aircraft drivetrains, removing the second vibration mode which is not present in all the drivetrain. Furthermore, this paper shows that the fuel pump modelled in [3] can be integrated in the gearbox model, which allows reducing the implementation model while maintaining the number of frequencies. These reductions allow lowering the complexity of the model, the space used by the setup and the cost since less equipment is used.

On the other hand, to model the electrical system, the multilevel paradigm [24], shown in Fig. 2 can be used. Four modelling levels are presented: Component Level, Behavioural Level, Functional Level, and Architectural Level. The lower in the pyramid, the higher the details used in the model and the longer the time taken for a typical simulation run. To model the electromechanical interactions, the complete system is modelled using the Functional Level, in which components are modelled with a bandwidth of hundreds of Hz (200-300 Hz). At this level of modelling the transients associated with the switching of power electronics devices are not needed. For that reason, the aircraft EPS is modelled as a direct current EPS, to which loads are connected, as the one proposed in the MOET EU, CleanSky, and Airbus HVDC projects [25]. Moreover, since the torque applied by a direct current (DC) and alternate current (AC) machines are equivalent for the drivetrain, the synchronous generator normally used in aircraft [26] is modelled by a DC generator. The use of the DC generator allows the connection of the electrical loads without the need of using power converters between the machine and the system.

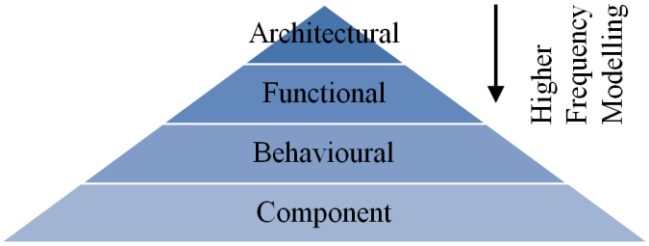

Fig. 2: Multilevel Modelling of Electrical Systems.

Furthermore, normally to experimentally measure the torsional vibrations, torque transducers and encoders are used. These sensors need to be installed in the middle of the shaft, increasing the system complexity, cost and space. Past studies [23, 27] have developed sensorless methods that allow the measurement of the speed of the system. However, to test its validity, sensors need to be installed. This paper introduces a sensorless methodology to measure the torsional vibrations, which is validated without the use of torque transducers.

This paper aims to demonstrate the electromechanical interaction due to the connection of electrical loads using a reduced electromechanical system model. The following contributions are presented in this paper:

- A two natural frequencies reduced mechanical drivetrain model that allows the study of electromechanical interaction in an aircraft while reducing the number of mechanical loads connected (in comparison to past studies), and hence decreasing the space and cost, is developed.
- A simplified electrical system that allows the study of the connection of electrical loads and its excitation of torsional vibrations is implemented. The system models the DC aircraft EPS and removes the power converters using a DC generator instead of a synchronous machine.
- A sensorless methodology to measure torsional vibrations is presented. In this paper, a sensorless method for high noise systems and a methodology to verify the sensorless method without the use of sensors are introduced.

The paper is organised as follows. In Section 2, the reduced model to study the electromechanical system is presented. The results are compared with those obtained in previous studies. In Section 3, the electromechanical interaction produced by the connection of electrical loads is demonstrated using the designed model. In Section 4, a sensorless methodology to measure the torque of the electromechanical system is introduced. In Section 5, the experimental results are presented and finally in Section 6 the conclusions are drawn.

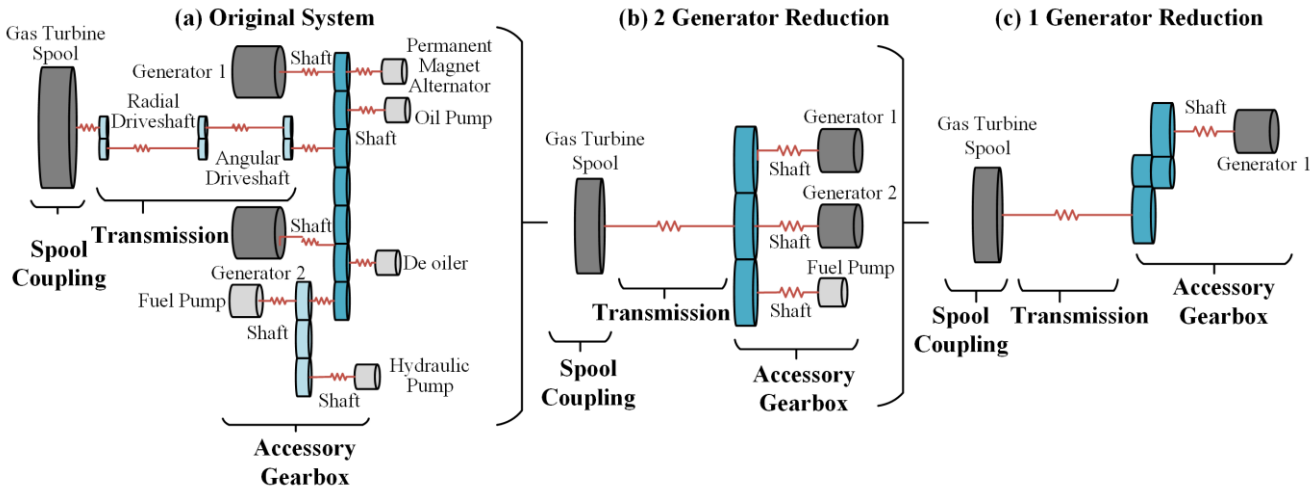

Fig. 3: Drivetrain Reduction

2. Modelling of The Reduced Electromechanical Interaction System

In this section, a reduced model to study the electromechanical interaction is presented. As shown in Fig. 1, the electromechanical system is composed of the engine, the drivetrain, the generator, and the EPS. Since the speed of the drivetrain is fixed by the engine in an aircraft [3], it is represented by a 2.2 kW induction machine operating at a constant speed with V/f control. The drivetrain, generator and EPS are described next.

2.1. Drivetrain Model

The mechanical system can be represented as a lumped mass system [3] as shown in Fig. 3. The machines, gears, and mechanical loads are symbolised as inertias, which are represented by the grey and blue disks. The couplings and shafts, shown in red, are characterised by their stiffness and damping. In Fig. 3(a), the drivetrain of an aircraft is shown. The connection point to the engine is the spool coupling (intermediate-pressure spool or high-pressure spool for three and two spool turbines configuration respectively [3]), which is connected through a transmission train, formed by a radial and angular driveshaft, to a gearbox. To this gearbox, mechanical loads (oil pump and de-oiler), an auxiliary load gearbox (to which fuel pump and hydraulic pump are coupled), and the two generators are connected.

The studies presented in [3, 23] showed that the main natural frequencies of the aircraft drivetrain of Fig. 3(a) are 26.6 Hz, 37.2 Hz, and 87.2 Hz. Moreover, the study identified that while the first and third mode were found all over the drivetrain, the second mode only appeared at the generators shaft. The second mode represented the out of phase movement between the two generators, and since the generators and their shaft are identical, the vibrations on them do not spread to the rest of the drivetrain. Also, in [3] was shown that the third mode was excited considerably less than the first one. Furthermore, the studies carried out in [3] showed that the components with greater inertia values, such as the generators, the engine spool, and the fuel pump were responsible for the value of the natural frequencies. With this information, [3, 23] and since the first vibration modes are the ones that produce the wear of the shaft, the model of Fig. 3(a) can be reduced to the system of Fig. 3(b) and still be representative of the aircraft drivetrain. Therefore, in the reduction presented in [3, 23] only the inertias responsible for the first three natural frequencies below 100 Hz are modelled. The drivetrain has been reduced to an engine represented by a motor, which is connected through a single shaft to a gearbox. To this gearbox, the two generators and an accessory load are connected.

The work presented in this paper aims to reduce the aircraft drivetrain model further and hence develop a simpler prototype that allows the study of the electromechanical interaction, while reducing the size, complexity and cost. As mentioned in [3], the second frequency mode is present only in the generators shaft since it is associated to the out of tune movement of the generators. Likewise, since the fuel pump inertia is connected directly to the gearbox and because its value is much lower than the generator one, the model developed in this paper integrates the fuel pump in the gearbox. Fig. 3(c) shows the drivetrain reduction introduced in this paper, in which one of the generators and the fuel pump of the reduction presented in [3, 23] have been removed. Therefore, in the reduced mechanical system, the engine of the system is connected to one generator through a drivetrain, while maintaining two natural frequencies below 100 Hz and dynamic behaviour like that of an aircraft drivetrain as is shown next.

The experimental drivetrain consists of three shafts rotating at different speeds, one connected to the prime mover, a middle shaft rotating at a faster speed, which is used for other experiments, and one connected to the generator as shown in Fig. 4. The ratio between shafts is 1:3:1.5, with the motor shaft the slowest and the central shaft the fastest. The gears used to change the speed are positioned as follows: Gear J_3 in the motor shaft, gears J_4 and J_5 in the middle shaft, and gear J_6 in the generator shaft. Flywheels are connected next to each machine to obtain aircraft drivetrain mechanical natural frequencies under 100 Hz.

To model the system, the state of each inertia is given by (1), where J_i represent the inertia value in kgm^2, θ_i, $\dot{\theta}_i$, $\ddot{\theta}_i$

are the angle in rad, the speed in rad/s, and the acceleration in rad/s^2 of the inertia, and $T_{(i-1),i}$ and $T_{i,(i+1)}$ are the torque applied and transmitted by the inertia. The index i is shown in Fig. 4.

$$J_i\ddot{\theta}_i = T_{(i-1),i} - T_{i,(i+1)} \quad (1)$$

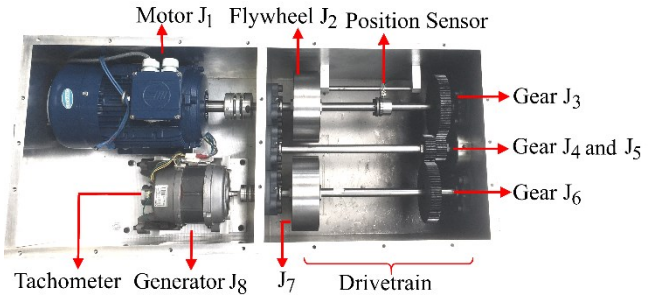

Fig. 4: Mechanical Setup.

In the case of the engine, which is represented by a motor, $T_{0,1} = T_m$, where T_m is the torque produced by the machine. Instead, for the generator $T_{8,9} = T_e$, where T_e is the electrical torque needed by the machine to produce the electrical power, which value is proportional to the resistive load connected. The rest of the torques on the system are proportional to the difference of speed and angle at the ends of each shaft and coupling and are given by (2). $k_{i,(i+1)}$ and $d_{i,(i+1)}$ represent the stiffness and damping of each shaft or coupling between inertias i and $i+1$.

$$T_{i,(i+1)} = k_{i,(i+1)}(\theta_i - \theta_{i+1}) + d_{i,(i+1)}(\dot{\theta}_i - \dot{\theta}_{i+1}) \quad (2)$$

Applying these two equations to the one-generator reduction of Fig. 3(c), the lumped mass system of (3) is found, where the inertia matrix is called J, the damping matrix D, and the stiffness matrix K. The states associated with the gears (inertias 3, 4, 5, and 6) have been reduced since the connection is not flexible and $\dot{\theta}_3 = 2/3\ \dot{\theta}_6$, $\dot{\theta}_4 = 2\dot{\theta}_6$, and $\dot{\theta}_5 = 2\dot{\theta}_6$. The value of the motor and generator torques are the inputs of the system and allow the connection to the electrical system. The real stiffness and inertias values of the shaft, flywheels, and gears were calculated from the experimental parameters using equations (4) and (5) respectively. With ρ the density of the material, L the length, r_o and r_i the external and internal radio respectively, and G the material shear modulus. The coupling stiffness and machines inertias were obtained from their datasheet. The obtained values referred to the generator are given in Table 1. The damping of each component is not given since accurate values are difficult to obtain experimentally [23]. The damping associated to each natural frequency has been determined experimentally in Section 5.

Solving the lumped mass system, the torsional vibrations modes are obtained. Their values if no flywheels are connected are 0 Hz, 103.82 Hz, and 339.13 Hz. These natural frequencies are higher than 100 Hz, and thus they are not representative of an aircraft drivetrain. Therefore, to obtain torsional vibrations below 100 Hz, two flywheels are connected to the system as shown in Fig. 4. Solving the same system with the two flywheels (diameter of 170 mm and a length of 60 mm), the torsional vibration modes obtained are 0 Hz, 35.99 Hz, and 82.15 Hz. Hence, when the flywheels are connected, the drivetrain has features similar to those of the aircraft engine driveshaft, with frequencies close to the 26.6 Hz, 37.2 Hz, and 87.2 Hz, which were proved in [3] to be representative of an aircraft drivetrain.

$$J = \frac{\pi\rho L}{2}(r_i^2 + r_o^2) \quad (4)$$

$$k = \frac{G\pi r_o^4}{2L} \quad (5)$$

To understand the effect of each vibration mode on the overall system, their behaviour is graphically studied as shown in Fig. 5. The circles symbolise the inertias, the shafts are shown in red, and the gearbox in blue. The vertical green lines represent the inertias referred angles in each natural frequency mode. In the first mode or rigid mode (0 Hz), the system moves together. In the second mode (35.99 Hz), the generator and motor are moving out of phase. In the third mode (82.15 Hz), the generator and motor move together while the gearbox moves in opposite direction.

Table 1 Parameters of the Drivetrain.

Parameter	Value
Gearbox Ratio	1.5
Referred Motor Inertia	$J_1 = 0.0026$ Kgm^2
Referred Motor Flywheel Inertia	$J_2 = 0.0172$ Kgm^2
Gears Inertia	$J_{3+4+5+6} = 0.0151$ Kgm^2
Generator Flywheel Inertia	$J_7 = 0.0386$ Kgm^2
Generator Inertia	$J_8 = 0.0005$ Kgm^2
Referred Motor Coupling Stiffness	$k_{12} = 50403$ Nm/rad
Referred Motor Shaft Stiffness	$k_{23} = 959.9111$ Nm/rad
Generator Shaft Stiffness	$k_{67} = 2239.8$ Nm/rad
Generator Coupling Stiffness	$k_{78} = 113406$ Nm/rad

To understand which vibration mode is being reduced, the torsional vibration modes presented in Fig. 5 are compared with the ones obtained for a two-generator reduced system. The two-generator system is designed for the same parameters of the one-generator system with the inertia, stiffness, and damping of the second generator equal to the ones of the first. The results obtained are shown in Fig. 6. Modes 1, 2 and 3 of the one-generator model are equivalent to the modes 1,2 and 4 of the two-generator system: Movement of the whole rig as one, out of phase

$$\begin{bmatrix} J_1 & 0 & 0 & 0 & 0 \\ 0 & J_2 & 0 & 0 & 0 \\ 0 & 0 & J_{3,4,5,6} & 0 & 0 \\ 0 & 0 & 0 & J_7 & 0 \\ 0 & 0 & 0 & 0 & J_8 \end{bmatrix} \begin{bmatrix} \ddot{\theta}_1 \\ \ddot{\theta}_2 \\ \ddot{\theta}_6 \\ \ddot{\theta}_7 \\ \ddot{\theta}_8 \end{bmatrix} + \begin{bmatrix} d_{12} & -d_{12} & 0 & 0 & 0 \\ -d_{12} & d_{12}+d_{23} & -d_{23} & 0 & 0 \\ 0 & -d_{23} & d_{23}+d_{67} & -d_{67} & 0 \\ 0 & 0 & -d_{67} & d_{67}+d_{78} & -d_{78} \\ 0 & 0 & 0 & -d_{78} & d_{78} \end{bmatrix} \begin{bmatrix} \dot{\theta}_1 \\ \dot{\theta}_2 \\ \dot{\theta}_6 \\ \dot{\theta}_7 \\ \dot{\theta}_8 \end{bmatrix} + \begin{bmatrix} k_{12} & -k_{12} & 0 & 0 & 0 \\ -k_{12} & k_{12}+k_{23} & -k_{23} & 0 & 0 \\ 0 & -k_{23} & k_{23}+k_{67} & -k_{67} & 0 \\ 0 & 0 & -k_{67} & k_{67}+k_{78} & -k_{78} \\ 0 & 0 & 0 & -k_{78} & k_{78} \end{bmatrix} \begin{bmatrix} \theta_1 \\ \theta_2 \\ \theta_6 \\ \theta_7 \\ \theta_8 \end{bmatrix} = \begin{bmatrix} T_m \\ 0 \\ 0 \\ 0 \\ -T_e \end{bmatrix} \quad (3)$$

movement of the two machines, and movement of the two machines opposite to the gearbox. Mode 3 of the two-generator system is reduced in the one-generator model since in [3] was shown that it is not present all over the drivetrain. This allows the removal of one generator.

Since the vibration modes of the two systems are equivalent, and because the frequencies are close to the ones presented in [3], the reduction model of one-generator has features like those of the aircraft drivetrain for the electromechanical interaction. Moreover, in the experimental system presented in [3] the vibration modes have been scaled down to 13 Hz and 22 Hz, while in this model values 35.99 Hz and 82.15 Hz which are closer to the 26.6 Hz and 87.2 Hz of the aircraft drivetrain are used.

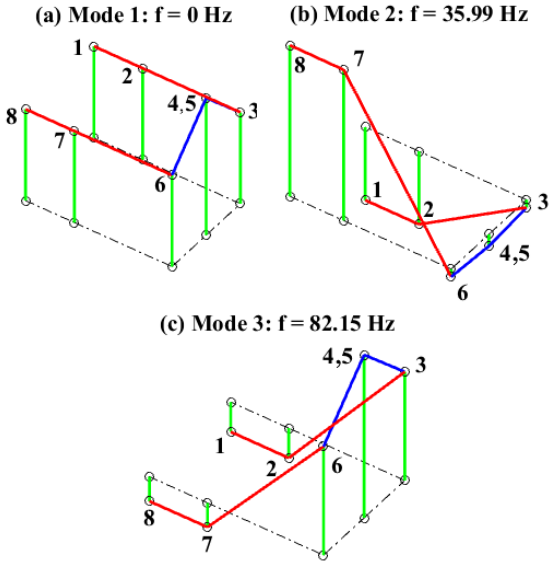

Fig. 5: Torsional Vibration Modes of One-Generator Reduction.

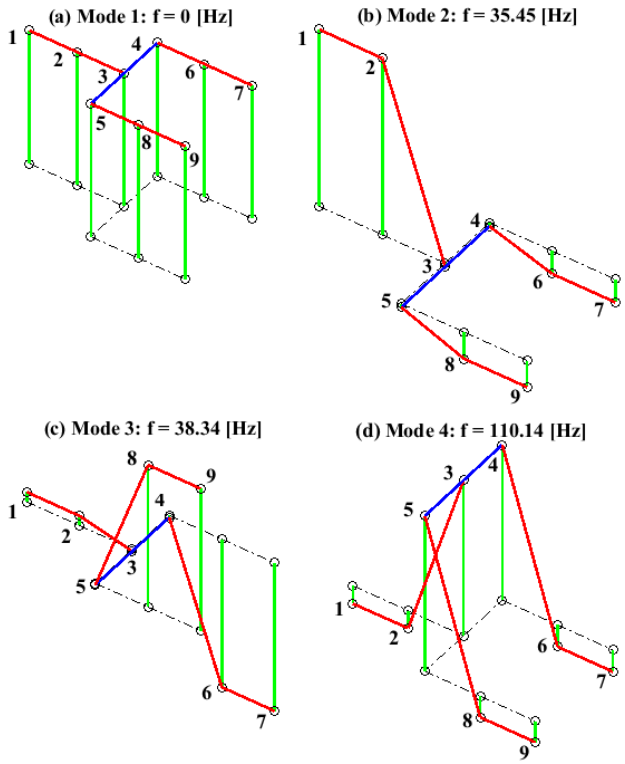

Fig. 6: Torsional Vibration Modes of Two-Generator Reduction.

2.2. *Electrical Power System Model*

The generator of an aircraft produces AC three-phase electrical power which can directly feed loads [7] or be rectified to feed a 270 V DC bus [28]. While previous architectures preferred the use of AC transmission systems, the EPS proposed by projects MOET EU, CleanSky, and Airbus HVDC [25] work in DC. For that reason, in the model presented in this paper the electrical loads are feed through a DC system. Furthermore, since the electrical system is modelled using the Functional Level, the switching of the converters is not modelled, and thus the rectifier stage is simplified, and the loads are feed directly by a 1 kW DC generator. This reduced model is easier to implement than the three-phase model previously developed in [3] and is representative of an aircraft EPS. Also, because from a control point of view, the torque applied to a drivetrain by a DC or AC generator are equivalent, the electromechanical interaction is not affected. Fig. 7 shows the diagram of the EPS.

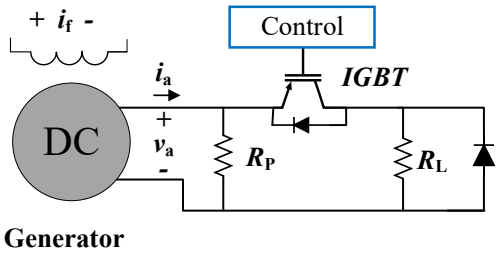

Fig. 7: Electrical System Reduction.

The generator used experimentally is a single phase 1 kW Nidec Universal Motor, which windings have been reconnected to operate as a DC generator with independent field. The generator is operating with constant field because for testing the electromechanical interaction a control system to keep the voltage constant is not needed. The machine equations are given by (6)-(9), in which T_e is the electrical torque needed by the machine to feed the load R_L, k is the rotational inductance, i_f is the field current, i_a is the armature current, E is the back electromotive force (EMF), v_a is the armature voltage at the terminals of the machine, R_a and L_a are the armature resistance and inductance respectively, V_0 is the voltage drop in the machine brushes, $\dot{\theta}_8$ is the speed of the generator, and R_{eq} is the load resistance obtained from R_P and R_L.

$$T_e = k i_f i_a \tag{6}$$

$$E = R_a i_a + L_a \frac{di_a}{dt} + V_0 + v_a \tag{7}$$

$$E = k i_f \dot{\theta}_8 \tag{8}$$

$$v_a = R_{eq} i_a \tag{9}$$

The EPS is represented by one resistance R_L that can be switched on/off by an insulated-gate bipolar transistor (IGBT), as shown in Fig. 7. To protect the machines and IGBT from the currents produced by the inductances when

the resistance is disconnected the following precautions are used:

- To protect the generator and dissipate the current when the IGBT turns off, a high resistance R_P is connected in parallel to machine output.
- To protect the IGBT when the switches are off, a diode has been connected in parallel to the load R_L.

The electrical and mechanical systems interact through the torque T_e and the generator speed $\dot{\theta}_8 = \omega_8$. Their values change proportionally to the load R_L connected The electrical system parameters are shown in Table 2 and the experimental setup is shown in Fig. 8.

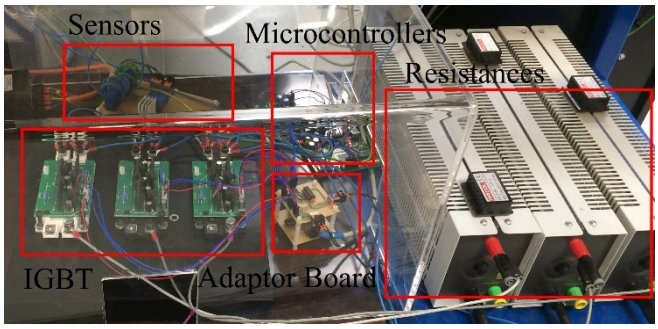

Fig. 8: Electrical Components.

Table 2 Parameters of the Electrical System.

Parameter	Value
Armature resistance	$R_a = 4.025\ \Omega$
Protection Resistance	$R_P = 60\Omega$
Rotational inductance	$k = 0.1274$ H
Drop Voltage Brushes	$V_0 = 12.247$ V
Armature Inductance	$L_a = 0.019$ H

2.3. Electromechanical System Model

The integration of the mechanical and electrical systems is achieved by combining the mechanical model from (3) and the electrical equations shown in (6)-(9). These two systems are related through the generator torque, which, as shown in (3), is an input of the mechanical drivetrain.

Then, first the state space representation $\dot{X}_{DT} = A_{DT}X_{DT} + B_{DT}U_{DT}$ of the mechanical drivetrain is obtained as shown in (10). The states of the system are the rotational angles θ_j and the rotational speed $\dot{\theta}_j$ of each inertia; and the inputs are the torques applied by the generators T_e and the engine T_m.

$$X_{DT} = [\theta_1, \theta_2, \theta_6, \theta_7, \theta_8, \dot{\theta}_1, \dot{\theta}_2, \dot{\theta}_6, \dot{\theta}_7, \dot{\theta}_8]^T$$

$$A_{DT} = \begin{bmatrix} 0 & I \\ -J^{-1}K & -J^{-1}D \end{bmatrix} B_{DT} = \begin{bmatrix} 0 \\ J^{-1} \end{bmatrix} U_{DT} = \begin{bmatrix} 0_{5,1} \\ T_m \\ 0 \\ 0 \\ 0 \\ -T_e \end{bmatrix} \quad (10)$$

Finally, the electromechanical system model introduced in this paper is given by $\dot{X} = AX + BU$, in which the matrix values are presented in (11).

$$A = \begin{bmatrix} A_{DT} & 0 \\ \begin{bmatrix} 0 & \frac{ki_f}{L_a} \end{bmatrix} & -\frac{1}{L_a}(R_a + R_{eq}) \end{bmatrix}$$
$$B = \begin{bmatrix} 0 \\ J^{-1} \end{bmatrix} U = \begin{bmatrix} U_{DT} \\ V_0 \end{bmatrix} X = \begin{bmatrix} X_{DT} \\ i_a \end{bmatrix} \quad (11)$$

3. Electromechanical Interaction Analysis

The electromechanical system described is modelled in PLECS®, and the interaction produced by the connection of electrical loads in the drivetrain is presented. The value of the inertias and stiffness associated with the generator, motor, gearbox, couplings and shaft of the described system are given by the parameters of the experimental components presented in Table 1 and Table 2. Fig. 9 shows the system response of the shaft when $R_L = 4.7\ \Omega$ is connected. In (a) the armature v_a (in blue) and the field voltage v_f (in red) are shown, while in (b) the constant field of $i_f = 6.2$ A (in red), and the armature current i_a (in blue) are depicted. The generator speed ω_8 is presented in (c), and in (d) the electrical torque T_e (in blue) and the generator shaft torque $T_{6,7}$ (in red) are displayed. The steady state value before and after the connection of the voltage, current, power and torque are shown in Table 3.

Fig. 9 (d) shows that a step connection T_e produces a transient vibration in the generator's side shaft $T_{6,7}$. These vibrations can decrease the life of the shaft producing fatigue.

Table 3 Steady State Parameters

Parameter	Value	
	Before Connection	After Connection
Armature Current	0.83 A	6.75 A
Armature Voltage	53.51 V	29.55 V
Electrical Power	44.41 W	199.46 W
Electrical Torque	0.37 Nm	2.97 Nm

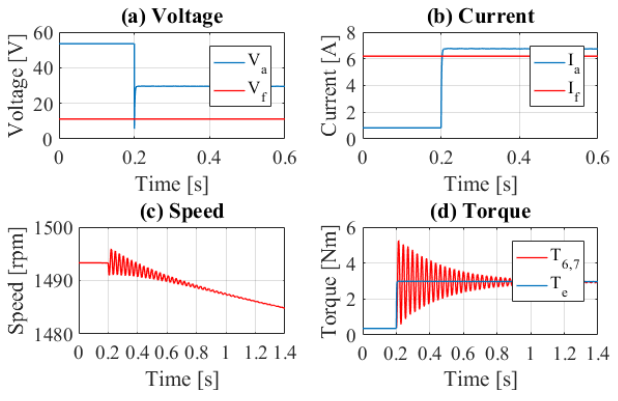

Fig. 9: Step Connection.

The frequency of the vibrations is obtained through Fast Fourier Transform (FFT) analysis of $T_{6,7}$, as shown in Fig. 10. It is observed that the torsional frequencies, for which the system was designed (35.99 Hz and 82.15 Hz), are being excited by the connection of the electrical load. Moreover like in the aircraft drivetrain shown in [3], the excitation of the mode associated to 82.15 Hz is much

smaller than the one of 35.99 Hz. Therefore, the model developed in this paper is consistent with the aircraft drivetrain.

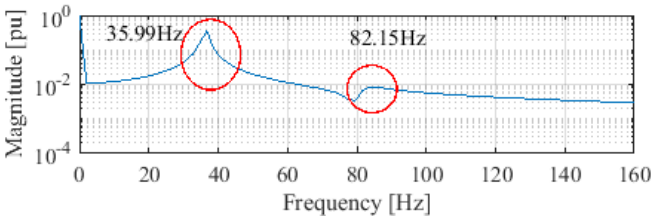

Fig. 10: FFT of System.

To further analyse the effect of the connection of electrical loads on the mechanical drivetrain, pulsating loads are connected as shown in Fig. 11. In blue the torque T_e is shown, and in red, the shaft torque $T_{6,7}$ is depicted. Fig. 11 (a) shows the step connection, while Fig. 11(b) and (c) show the connection of pulsating loads with low and high frequencies respectively. In Fig. 11(d) the connection of an ununiformed pulse is shown. It is observed that the connection of pulsating loads affects the excitation of the torsional vibrations differently. While the connection of a low-frequency pulse excites multiple times the drivetrain, a high-frequency pulse is perceived as a step connection. Moreover, the connection of the ununiformed pulse shows that the timing of the pulse connection can reduce the excitation of the torsional vibrations.

Since load connections excite the torsional vibrations differently depending on their frequency, the study of the electromechanical interaction due to electrical load connections is fundamental. The reduced model presented in this paper allows the analysis of these vibrations using a simple straight forward model, that can connect electrical loads with different switching frequencies.

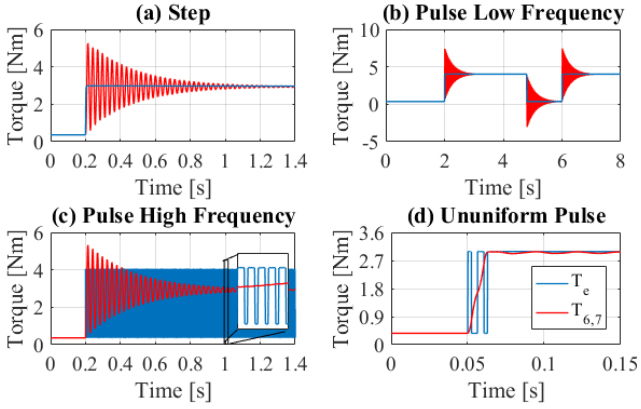

Fig. 11: Excitation of Torsional Frequencies.

4. Sensorless Measurement

In most cases, it is possible (but undesirable) to install a torque transducer on a drivetrain. These sensors are expensive and require large installations [29], adding complexity to the reduced model in the study. Moreover, the transient detection of the sensors, which is fundamental for the study of the electromechanical interaction, depends on its level of accuracy. The use of sensorless control avoids this problem and allows the reduction of hardware complexity, cost and size [29].

However, in practice when developing experimental sensorless methods they must be tested against sensor results to check its accuracy [23, 27]. This counters one of the main advantages of sensorless methods, when the method is developed for experimental models: because the rig in which the sensorless strategies are applied must have sensors, complexity, cost and sometimes even size is added to the setup. This paper introduces a methodology to test a sensorless method without the need for sensor data, and hence effectively reduce the complexity, space and cost of the experimental setup.

The methodology developed in this paper is composed of five steps which are explained next:

- First the experimental parameters are measured.
- Second the experimental parameters are used in the system model implemented in software such as PLECS® or Simscape®.
- Third the sensorless method to measure torque using electrical parameters is developed. This method is tested against the torque obtained by simulation, using the simulation electrical results, such as current and voltage, to which noise has been added to represent real experimental data.
- Fourth, once the sensorless strategy is accurate, the method is experimentally implemented.
- Finally, the sensorless experimental results are tested against the simulation ones to validate the strategy. Since the simulation has used experimental parameters, both results are compared and the sensorless method validated.

Most sensorless measuring methods are based on estimation technics or mathematical models. Mathematical model methods obtain the angle and speed of the system by estimating the back-EMF and are typically used for medium and high-speed systems [30]. When operating at low speeds, the back-EMF presents large errors, because the voltage drop in the stator resistance is high compared to the EMF. For this reason, in low-speed systems estimation methods are used. For example, in [29, 31] the resistance of the system must be estimated using high frequency signals. Moreover, for DC and synchronous machines working at medium and high speed the back-EMF can be easily obtained using the system performance [23, 30, 32]. Another aspect to consider when choosing sensorless methods is the accuracy needed in the system. While steady state performances are easy to obtain, as shown in [29, 33], the analysis of transient responses can be concealed by noise [27, 29, 34]. For that reason, the sensorless strategy will depend on the machine used, the system speed, the accuracy needed, and the noise in the system.

In general, it is not desired to work with systems that require high knowledge of its components. However, in this experimental setup, since the operation speed is high and the DC machine parameters are known, a model based back-EMF strategy that uses the measured values of v_a, i_a, and i_f is employed. Also, since as shown in Fig. 11, the electromechanical interaction is observed in the transient response, the back-EMF method developed in this paper is combined with signal filtering to eliminate the noise of the signals. Experimentally, these signals are obtained using current and voltage transducer sensors model LA100-P and LV25-P respectively, which are connected to dSpace using

an acquisition frequency of 10 kHz. Moreover, since the aim of the model developed in this paper is to reduce the experimental setup complexity, the system does not have a torque transducer installed. Therefore, the sensorless strategy is validated using the proposed sensorless methodology.

As explained in the methodology, first the experimental parameters are measured, and then, they are used in the simulation implemented in PLECS®. These parameters were presented in Table 1 and Table 2. Then, because the experimental data has high noise, to emulate the real results, white noise is added to the armature voltage v_a, armature current i_a, and to the field current i_f obtained by simulation and shown in Fig. 9. The resulting noisy data is employed in the proposed sensorless strategy. The results obtained will be compared with the simulation torque and in Section 5 with the experimental data obtained to validate the method.

The rest of the section describes steps third and fourth of the sensorless methodology: First, a resonant filter to eliminate the noise of the signals is presented. Later, the speed of the system and the torque are calculated and compared with the simulation data.

4.1. Filtering of the Data

Bandpass resonant filters are used to remove the noise of the measured v_a, i_a, and i_f, and thus obtain only the components associated with the torsional vibration response. The frequencies of the torsional vibrations are then obtained applying FFT to i_a or v_a. Then, the measured signals are filtered at each natural frequency using the resonant filter of (12). Where, f_0 is the frequency of the bandpass filter, and q is the quality factor given by $q = f_0/df$ with df the bandwidth. To obtain only the components associated to one frequency, and effectively remove the noise, bandpass resonant filters operate with small bandwidths.

$$H(s) = \frac{2\pi\frac{f_0}{q}s}{s^2 + 2\pi\frac{f_0}{q}s + (2\pi f_0)^2} \tag{12}$$

After applying the resonant filter for each torsional frequency value to the measured signal s_m, the reconstructed signal s_T without noise is given by (13). The signal s_T is formed by the sum of the DC value of the measured signal $s_m(\mathrm{DC})$ and the values of the signal at each natural frequency $s_m(f_i)$. To eliminate the filter response to a step connection $s_F(f_i)$, its value is subtracted. The component p_i represents the participation of the frequency in the total signal, and its value is given by the normalized magnitude of the FFT response of the step connection.

$$s_T = s_m(\mathrm{DC}) + \sum_{i=1}^{i=n} p_i\left(s_m(f_i) - s_F(f_i)\right) \tag{13}$$

Using the PLECS® results with added noise, the measurement signals are filtered for the frequencies $f_1 = 35.99$ Hz and $f_2 = 82.15$ Hz given in Fig. 10, using a bandwidth of 1 Hz. This bandwidth was chosen to filter the noise and obtain signals with natural frequencies with magnitude equal to the original. The participation factor p_1 and p_2 are obtained from the power spectrum of Fig. 10: $p_1 = 0.3377$ and $p_2 = 0.0065$.

4.2. Torque Determination

The speed ω_8 must be calculated to obtain the torque of the system. For a DC machine, its value in rad/s can be obtained from the back-EMF using (8). The value of k and i_f are constant and the induced voltage, E, depends on the filtrated v_a and i_a, as shown in (7). Neglecting the friction on the system, the torque of the generator shaft can be calculated by (14). The electrical torque, T_e, gives the steady state value and is obtained from (6). The transient torque, $T_{transient}$, produces the vibrations of the system and is calculated as shown in (15).

$$T_{shaft} = T_e + T_{transient} \tag{14}$$

$$T_{transient} = J_g\dot{\omega}_g \tag{15}$$

Following the described steps: filtering the noise of the signal, calculating the speed, and calculating the torque, the torque on the shaft is obtained. Fig. 12 shows the torque given by the simulation in PLECS® (in blue), and the torque obtained with the described sensorless method (in red) for the four electrical load connections presented in Section 3. It is observed that the results achieved are the same for the transient response, while for the steady-state response, the sensorless measurement presents low vibrations around the steady-state value, which are due to noise in the signals and filters.

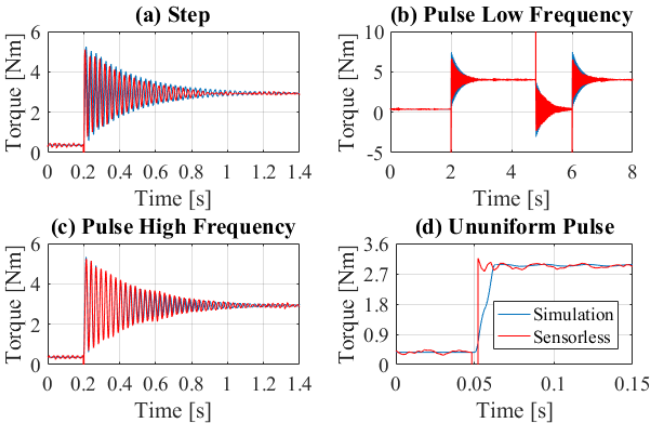

Fig. 12: Sensorless Torque Measurement.

To study the effectiveness of the method, the FFT of the estimated signals is compared with the FFT of the simulation results. Fig. 13 shows that the normalised estimated FFT (in red) and the simulation FFT (in blue) have the same peak values. Since the magnitude of the peak frequencies of the filtered signal is equal to the original signal without noise, the bandwidth of the resonant filter allows the removal of most of the noise while maintaining the torsional frequencies value. However, since the sensorless signals have some remaining noise, some other frequencies are also present. This noise appears higher in the case of the ununiformed pulse since the torsional vibrations are not being excited, and hence, the noise is proportionally higher.

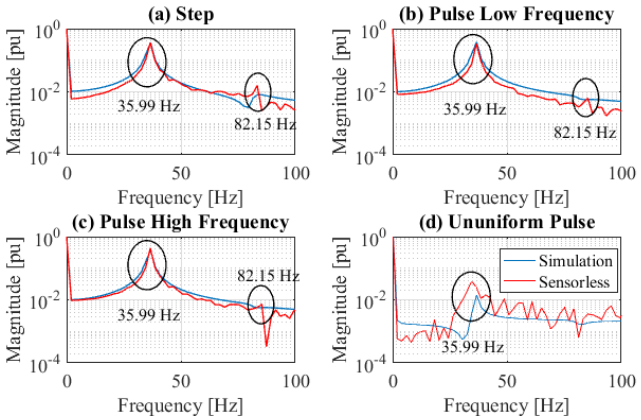

Fig. 13: Sensorless FFT.

From the time domain results and the FFT analysis, the sensorless measurement proposed appears like a valid method for the analysis of the transient torque response on the described electromechanical interaction system. The validation of the method against experimental data is presented in the next section.

5. Experimental Results

In this section, first, the test rig is characterised regarding its critical speeds and torsional frequencies. Then, the electromechanical interaction is demonstrated and the sensorless strategy verified.

5.1. Critical Speeds

Critical speeds or transversal vibrations increase the displacement of the rotating components of a drivetrain and are excited when the shaft rotational speed is equal to the critical speeds [1]. To measure the critical speeds, the motor shaft displacement is measured for rising values of it. The shaft displacements are measured using a contactless position sensor, Lion Precision model U5C, which is shown in Fig. 4 and measures the motor shaft movements along the x and y-axis. The steady-state speed is measured using a tachometer incorporated in the generator. The tachometer produces a sinusoidal wave with a frequency proportional by 7.5 to the generator speed. To get the speed of the motor shaft, the generator speed is obtained and divided by 1.5, the ratio of the speed between the shafts.

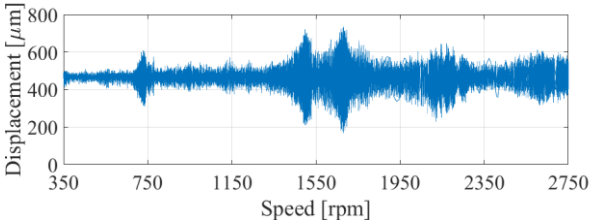

Fig. 14: Critical Speed Identification.

Fig. 14 shows the displacement of the shaft connected to the motor for ascending speed. Higher displacements show higher vibrations. Therefore, the critical speeds are those at which the vibrations are highest: 733 rpm, 1497 rpm, 1669 rpm, 2170 rpm, and 2631 rpm.

5.2. Torsional Vibrations

To experimentally identify the torsional vibration modes, the armature current i_a measured with a current transducer is analysed through FFT. Using 10 seconds of data after the application of an electrical load step connection with a sampling time $t_s = 10^{-5}$ s, and normalising the magnitude by the steady state value $i_a/i_{a_{steady}}$, the results shown in Fig. 15 are obtained. To observe the effect of the speed on the torsional vibrations, the results obtained at 1500 rpm (in (a)) and 2000 rpm (in (b)) in the generator shaft are presented. In black, the frequencies associated with the speed at which the system is run are enlighten: 1500 rpm = 25 Hz and 2000 rpm = 33 Hz. 50 Hz and 67 Hz are the speed in the middle shaft, which is used for experiments out of the scope of this paper.

At $f_1 = 35$ Hz and $f_2 = 74$ Hz small frequency variations are detected between the two results. Also, the peak detected at 74 Hz is lower than the one found at 35 Hz. This behaviour is consistent with the aircraft drivetrain described in [3], the model developed in Section 2, and the simulation results shown in Section 3. Furthermore, since the speed was controlled using V/f control, for 2000 rpm the FFT could not be calculated right after the step connection because the speed changes generated multiple speed harmonics. Consequently, both frequencies obtained at 2000 rpm are lower than those at 1500 rpm. This is particularly important for the peak at 74 Hz, which due to the noise of the signals is hard to detect. Nonetheless the frequency is considered since it can still be identified, because it is close to the design value, and since the behaviour is consistent with the model. Finally, repeating the FFT detection for different data set around 1500 rpm show that the torsional frequencies of the system are in the following ranges:

- $f_1 \in [35 - 37]$ Hz
- $f_2 \in [73 - 77.1]$ Hz

These differences are observed because an exact number of periods was not used for the FFT calculation, since there is more than one frequency present in the system. Moreover, the experimental system is sensible to variations such as load applied and flywheels position. Likewise, the backlash in the gears, which was not accounted for in the model, moves the torsional vibrations. Still, since the relative difference between the measurements is small (5.4% for f_1 and 5.1% for f_2), the values are considered acceptable. Also, the frequencies are close to the design values presented in Section 2: 35.99 Hz and 82.15 Hz.

To analyse further the behaviour of the system, the damping of each natural frequency is determined using the method presented in [35, 36], which consisted of combining the Hilbert Transformation with Empirical Mode Decomposition (EMD). The damping obtained are $\xi_1 = 0.018$ and $\xi_2 = 0.012$ associated to f_1 and f_2 respectively. These values confirm that the torsional vibrations are damped, and hence they have an exponential decay after being excited. This is consistent with the lower excitation of the frequencies at 2000 rpm.

Additionally, writing the torsional frequencies in the equivalent rpm it can be seen that 35 Hz equated to 2100 rpm. This value is one of the critical speeds, showing

that because of the gears the torsional vibrations produce transversal vibrations.

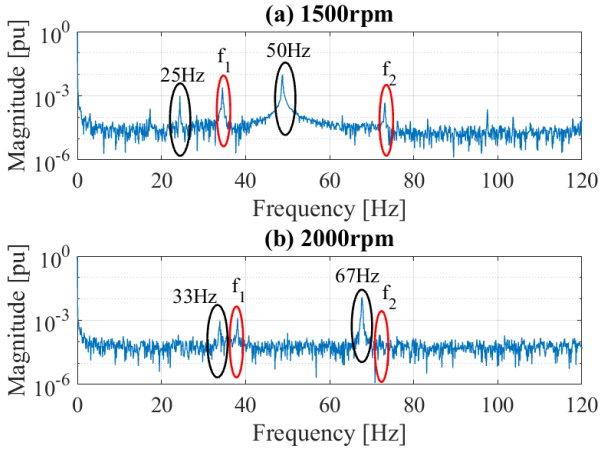

Fig. 15: Fourier analysis at Different Speed.

5.3. Electromechanical Interaction

Once the critical frequencies and the torsional vibration frequencies have been found, the electromechanical interaction of the system can be studied. Fig. 16 shows the experimentally measured currents i_{a} and i_{f}, armature voltage v_{a}, and the sensorless torque $T_{6,7}$ (in red), and in blue the corresponding simulation results obtained after a resistive load is connected.

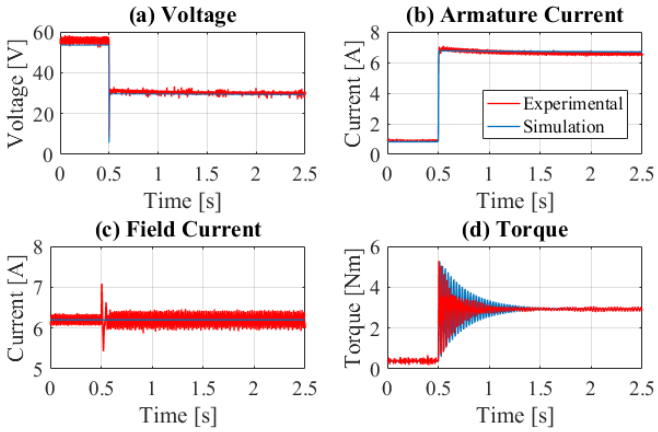

Fig. 16. Simulation and Experimental Data Comparison.

The system operates with a field current $i_{\mathrm{f}} = 6.2$ A and at a speed $\omega_8 = 1550$ rpm approximately. After the load is connected, the speed decreases to under 1500 rpm because the V/f control of the machine is not ideal. The load initially attached to the system is 0.3649 Nm, given by the resistance $R_{\mathrm{P}} = 60\ \Omega$. The final load in the system, after R_{L} has been connected, is 2.94 Nm. The torsional vibrations due to the load connection can be observed in Fig. 16(d).

The simulation and experimental results are very similar, so the experimental system has been well characterised, and the sensorless methodology has been validated. The differences obtained between simulation and experimental torque decay time show that the damping used by simulation was not the exact damping of the experimental system. This is because, as it was discussed in Section 2, only the damping of the experimental vibration modes could be determined and not the exact damping of each component.

Moreover, since the connection of electrical loads excites torsional vibrations, which are shown in the torque transient, the electromechanical interaction has been demonstrated. It has also been proven that the reduced model allows the study of the electromechanical interaction, and since the frequencies of the drivetrain are $f_1 \in [35 - 37]$ Hz and $f_2 \in [73 - 77.1]$ Hz, the system has drivetrain features similar to the ones of an aircraft engine presented in [3].

6. Conclusion

This paper presented a reduced model of an aircraft drivetrain which is used for the study of electromechanical interaction. The reductions introduced in this paper are:

- The drivetrain has been reduced from a two-generator and one load system to a one generator system, while maintaining the vibration modes present in all the aircraft drivetrain with values close to the real ones.
- The electrical system has been modelled as a DC system, representing the EPS of modern aircraft.
- The EPS has been further reduced by removing the switching of the aircraft rectifier. This was achievable changing the AC synchronous generator by a DC machine. For the drivetrain control, both machines are equivalent.
- A sensorless methodology has been presented, tested, and validated. The methodology allows the validation of the sensorless strategy without the need of sensors which add complexity to the drivetrain model.
- A sensorless torque measurement, that can work with noisy signals and that is based in the mathematical model of the DC machine, has been tested.

The reduced model allows the analysis of the torsional vibrations excited by electromechanical interaction in the machines shaft. Furthermore, the reduced EPS allows the study of electrical loads being connected with different switching frequencies and patterns. Thus, the reduced electromechanical system is representative of real systems in which loads can be pulsating and steps (among others).

Moreover, since simulation and experimental results are very similar, the simulation model can be used to analyse the electromechanical interactions in this type of system with a good degree of confidence.

7. References

1 Friswell, M.I., Penny, J.E.T., Garvey, S.D., Lees, A.W.: 'Dynamics of Rotating Machines' (Cambridge University Press, 2010)

2 Walker, D.N., Bowler, C.E.J.J., Jackson, R.L., Hodges, D.A., Bowler, C.E.J.J., Jackson, R.L.: 'Results of subsynchronous resonance test at Mohave'*IEEE Trans. Power Appar. Syst.*, 1975, **94**, (5), pp. 1878–1889.

3 Feehally, T., Damian, I.E., Apsley, J.M.: 'Analysis of Electromechanical Interaction in Aircraft Generator Systems'*IEEE Trans. Ind. Appl.*, 2016, **52**, (5), pp. 4327–4336.

4 Ying, J., Yuan, X., Hu, J., He, W.: 'Impact of Inertia Control of DFIG-Based WT on Electromechanical Oscillation Damping of

SG'*IEEE Trans. Power Syst.*, 2018, **33**, (3), pp. 3450–3459.
5 Fateh, F., White, W.N., Gruenbacher, D.: 'Torsional Vibrations Mitigation in the Drivetrain of DFIG-Based Grid-Connected Wind Turbine'*IEEE Trans. Ind. Appl.*, 2017, **53**, (6), pp. 5760–5767.
6 Ahumada S., C., Garvey, S., Yang, T., Wheeler, P.: 'Electric Load Impact over Shaft Connecting the Engine and Generator in More Electric Aircraft (MEA)', in 'SAE Technical Papers, in Press' (no date)
7 Wheeler, P.W., Clare, J.C., Trentin, A., Bozhko, S.: 'An overview of the more electrical aircraft'*Proc. Inst. Mech. Eng. Part G J. Aerosp. Eng.*, 2013, **227**, (4), pp. 578–585.
8 Kavil Kambrath, J., Wang, Y., Yoon, Y.-J., *et al.*: 'Modeling and Control of Marine Diesel Generator System With Active Protection'*IEEE Trans. Transp. Electrif.*, 2018, **4**, (1), pp. 249–271.
9 Erazo-Damian, I., Iacchetti, M.F., Apsley, J.M.: 'Electromechanical interactions in a doubly fed induction generator drivetrain'*IET Electr. Power Appl.*, 2018, **12**, (8), pp. 1192–1199.
10 Apsley, J.M., González-Villaseñor, A., Barnes, M., *et al.*: 'Propulsion drive models for full electric marine propulsion systems'*IEEE Trans. Ind. Appl.*, 2009, **45**, (2), pp. 676–684.
11 Tripathi, A., Narayanan, G.: 'Analytical Evaluation and Reduction of Torque Harmonics in Induction Motor Drives Operated at Low Pulse Numbers'*IEEE Trans. Ind. Electron.*, 2018, **66**, (2), pp. 967–976.
12 Ahumada, S.C.C., Garvey, S., Yang, T., Wheeler, P., Morvan, H.: 'The importance of load pulse timing in aircraft generation' (2015), pp. 1339–1345
13 Walker, D.N., Adams, S.L., Placek, R.J., Adams, L., Placek, R.J.: 'Torsional Vibration and Fatigue of Turbine-Generator shafts'*IEEE Trans. Power Appar. Syst.*, 1981, **PAS-100**, (11), pp. 4373–4380.
14 Bijami, E., Farsangi, M.M.: 'Robust hierarchical damping controller for uncertain wide-area power systems'*IET Gener. Transm. Distrib.*, 2018, **12**, (22), pp. 5958–5967.
15 Du, W., Bi, J., Wang, H.: 'Damping Degradation of Power System Low-Frequency Electromechanical Oscillations Caused by Open-Loop Modal Resonance'*IEEE Trans. Power Syst.*, 2018, **33**, (5), pp. 5072–5081.
16 Holdrege, J.H., Subler, W., Frasier, W.E.: 'AC Induction Motor Torsional Vibration Consideration - A Case Study'*IEEE Trans. Ind. Appl.*, 1983, **IA-19**, (1), pp. 68–73.
17 Joyce, J.S., Kulig, T., Lambrecht, D.: 'Torsional Fatigue of Turbine-Generator Shafts Caused by Different Electrical System Faults and Switching Operations' (1978), PAS-97, pp. 1965–1977
18 Valenzuela, M.A., Bentley, J.M., Lorenz, R.D.: 'Evaluation of torsional oscillations in paper machine sections'*IEEE Trans. Ind. Appl.*, 2005, **41**, (2), pp. 15–22.
19 Sheppard, D.J.: 'Torsional vibration resulting from adjustable-frequency AC drives'*IEEE Trans. Ind. Appl.*, 1988, **24**, (5), pp. 812–817.
20 IEEE: 'Proposed Terms and Definitions for Subsynchronous Oscillations'*IEEE Trans. Power Appar. Syst.*, 1980, **PAS-99**, (2), pp. 506–511.
21 Ran, L., Xiang, D., Kirtley, J.L., *et al.*: 'Analysis of electromechanical interactions in a flywheel system with a doubly fed induction machine'*IEEE Trans. Ind. Appl.*, 2011, **47**, (3), pp. 1498–1506.
22 Schmidt, P., Rehm, T.: 'Notch filter tuning for resonant frequency reduction in dual inertia systems', in 'Conference Record of the 1999 IEEE Industry Applications Conference. Thirty-Forth IAS Annual Meeting (Cat. No.99CH36370)' (IEEE, 1999), pp. 1730–1734
23 Moore, G.: 'Electro-Mechanical Interactions in Aerospace Gas Turbines'. University of Nottingham, 2012
24 Yang, T., Bozhko, S., Asher, G.: 'Functional Modeling of Symmetrical Multipulse Autotransformer Rectifier Units for Aerospace Applications'*IEEE Trans. Power Electron.*, 2015, **30**, (9), pp. 4704–4713.
25 Chen, J.J., Wang, C., Chen, J.J.: 'Investigation on the Selection of Electric Power System Architecture for Future More Electric Aircraft'*IEEE Trans. Transp. Electrif.*, 2018, **PP**, (99), p. 1.
26 Feehally, T., Apsley, J.M.: 'The Doubly Fed Induction Machine as an Aero Generator'*IEEE Trans. Ind. Appl.*, 2015, **51**, (4), pp. 3462–3471.
27 Darba, A., D'haese, P., De Belie, F., Melkebeek, J.A.: 'Improving the Dynamic Stiffness in a Self-Sensing BLDC Machine Drive Using Estimated Load Torque Feedforward'*IEEE Trans. Ind. Appl.*, 2015, **51**, (4), pp. 3101–3114.
28 Gao, F., Bozhko, S., Costabeber, A., Asher, G., Wheeler, P.: 'Control Design and Voltage Stability Analysis of a Droop-Controlled Electrical Power System for More Electric Aircraft'*IEEE Trans. Ind. Electron.*, 2017, **64**, (12), pp. 9271–9281.
29 Kumar, D., Radcliffe, P.: 'Sensorless speed measurement for brushed DC motors'*IET Power Electron.*, 2015, **8**, (11), pp. 2223–2228.
30 Li, H., Zheng, S., Ren, H.: 'Self-Correction of Commutation Point for High-Speed Sensorless BLDC Motor With Low Inductance and Nonideal Back EMF'*IEEE Trans. Power Electron.*, 2017, **32**, (1), pp. 642–651.
31 Liang, D., Li, J., Qu, R.: 'Sensorless Control of Permanent Magnet Synchronous Machine Based on Second-Order Sliding-Mode Observer With Online Resistance Estimation'*IEEE Trans. Ind. Appl.*, 2017, **53**, (4), pp. 3672–3682.
32 Nagorny, A.S.: 'A simple and accurate method for the experimental performance evaluation of high speed sensorless brushless dc motors', in '2009 IEEE International Electric Machines and Drives Conference' (IEEE, 2009), pp. 916–921
33 Darba, A., D'haese, P., De Belie, F., Melkebeek, J.: 'Rotor speed, position and load torque estimation using back-emf sampling for self-sensing brushless DC machine drives', in '2014 IEEE 5th International Symposium on Sensorless Control for Electrical Drives' (IEEE, 2014), pp. 1–7
34 Ahumada, C., Garvey, S., Yang, T., Wheeler, P.: 'Electromechanical interaction analysis through sensorless torque measurement', in '2017 IEEE Southern Power Electronics Conference (SPEC)' (IEEE, 2017), pp. 1–6
35 Lu, W., Du, X., Ding, J., Wang, X.: 'Modal parameter identification based on fast fourier transform and Hilbert Huang transform', in '2012 2nd International Conference on Consumer Electronics, Communications and Networks (CECNet)' (IEEE, 2012), pp. 2703–2706
36 Smith, C.B., Wereley, N.M.: 'Transient analysis for damping identification in rotating composite beams with integral damping layers'*Smart Mater. Struct.*, 1996, **5**, (5), pp. 540–550.